

Giant half-cycle attosecond pulses

H.-C. Wu^{1,*} and J. Meyer-ter-Vehn²

¹*Los Alamos National Laboratory, Los Alamos, New Mexico 87545, USA*

²*Max-Planck-Institut für Quantenoptik, D-85748 Garching, Germany*

(Dated: November 11, 2011)

Half-cycle picosecond pulses have been produced from thin photo-conductors, when applying an electric field across the surface and switching on conduction by a short laser pulse. Then the transverse current in the wafer plane emits half-cycle pulses in normal direction, and pulses of 500 fs duration and 10^6 V/m peak electric field have been observed. Here we show that single half-cycle pulses of 50 as duration and up to 10^{13} V/m can be produced when irradiating a double foil target by intense few-cycle laser pulses. Focused onto an ultra-thin foil, all electrons are blown out, forming a uniform sheet of relativistic electrons. A second layer, placed at some distance behind, reflects the drive beam, but lets electrons pass straight. Under oblique incidence, beam reflection provides the transverse current, which emits intense half-cycle pulses. Such a pulse may completely ionize even heavier atoms. New types of attosecond pump-probe experiments will become possible.

PACS numbers: 52.59.Ye, 42.65.Ky, 52.38-r, 52.65.Rr

A major goal of attosecond science [1] is to follow electron dynamics on the atomic time scale (24 as), be it in atoms or solids. Different methods to produce single attosecond pulses to this end have been described recently, and some of them have been tested experimentally [2]. These methods rely on the generation of high harmonics spectra which correspond to trains of as pulses in the time domain. Generating these spectra with few-cycle drive pulses and applying high-pass filters may be used to isolate single spikes. For pump-probe experiments, sufficiently intense pulses are required, and surface harmonics generated at solid-density plasma surfaces may provide high enough photon numbers [3].

In the present letter, we follow a very different route, producing half-cycle attosecond pulses from ultrathin relativistic electron sheets (RESs). We note that similar half-cycle pulses, radiated from current sheets in photo-conductors at rest, have actually been observed [4] and have been used in ionization experiments [5]. Another proposal is to produce disk-like, relativistic electron pulses from a synchrotron and to kick them sideward by a magnetic field; picosecond 200 MW half-cycle pulses are predicted this way [6].

The present work is based on two recent developments: (1) The generation of few-cycle high-contrast laser pulses at intensities exceeding 10^{19} W/cm² [7]. Making use of OPCPA techniques [8] and plasma mirrors [9], contrast ratios beyond 10^{10} (subpicosecond time intervals as required in this case) have been reached. High contrast is crucial to not destroy the ultra-thin targets foils prematurely. (2) The second innovation concerns the fabrication of few or even single carbon-atom layer graphenes [10, 11]. The graphene films are transparent to the laser light, even at electron densities of $n_e \approx 10^{24}$ cm⁻³ after full ionization. An outstanding feature here is that laser

pulses now available can blow out all electrons from these foils. This happens when the laser electric amplitude E_L is larger than the charge separation field $E_s = en_e d / \epsilon_0$, where ϵ_0 is the vacuum dielectric constant, d the thickness, and $en_e d$ the charge areal density of the foil. It is the $v \times B_L$ part of the laser interaction accelerates all electrons in laser direction. Relativistic energies up to a maximum of $\gamma = 1 + a_0^2/2$ are reached over a few micrometer; here $a_0 = E_L/E_0$ is the normalized field strength, $E_0 = mc\omega_L/e$ the normalizing field, ω_L the laser circular frequency, e and m electron charge and mass, and c the velocity of light. The electrons then form a thin RES, separated from the ions and surfing on the laser wave front [12].

These high-density sheets may serve as relativistic mirrors, compressing femtosecond probe pulses to attosecond pulses by Doppler shifts of $4\gamma^2$. For this to happen one has to divert the drive pulse from the RES by an additional foil that is just thick enough (≈ 50 nm) to reflect the light, but let the relativistic electrons pass almost unperturbed. Behind the reflector, the electrons propagate in field-free ($a = 0$) space, where, due to conservation of canonical momentum, also their transverse momentum ($p_\perp/mc = a$) vanishes. This means that the RES moves precisely in normal direction, i.e. the direction of the incident drive pulse. This makes it a perfect relativistic mirror for coherent Thomson backscattering [13].

Here we consider the same configuration, but now for oblique incidence of s -polarized laser light. A schematic drawing is given in Fig. 1 and a corresponding two-dimensional (2D) particle-in-cell (PIC) simulation in Fig. 2. The amazing new feature is the appearance of a strong half-cycle attosecond XUV/x-ray (HCX) electromagnetic pulse, preceding the RES after emerging from the reflector layer. This is the central new result of this paper. As we shall explain in the Methods section, the HCX pulse results from conservation of canonical momentum under the condition of oblique incidence. Due to interaction with the reflected laser pulse, each RES electron

*e-mail: hcwu@lanl.gov or huichunwu1@gmail.com

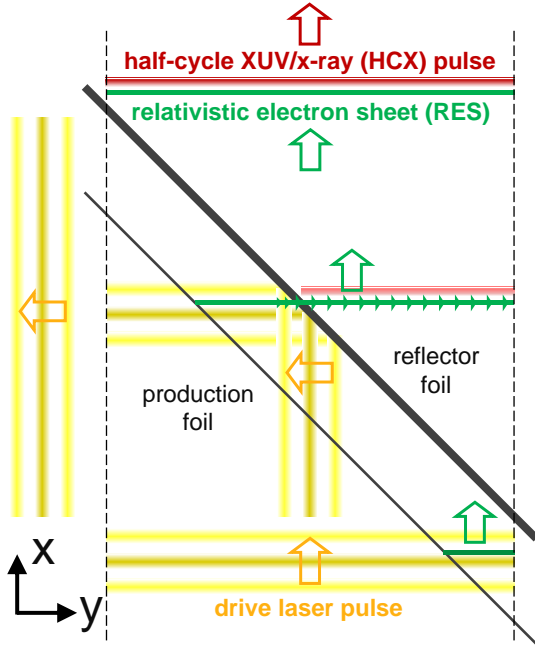


FIG. 1: **Scheme of target interaction and half-cycle emission.** A three-cycle, s -polarized laser pulse (central intensity maxima shown in yellow-brown) is obliquely incident on a double foil target. The drive laser pulse is shown at different times with yellow arrows showing propagation direction: (1) it starts passing the transparent electron production foil on the right-hand side, ionizing and accelerating electrons which then move (green arrows) as relativistic electron sheet (RES, green) parallel to the wavefront; (2) the drive pulse is reflected by the reflector foil, while the electron sheet is moving straight on; due to conservation of canonical momentum (see Methods section), electrons get a sudden transverse kick (indicated by small green arrows); the corresponding unilateral current radiates a short half-cycle XUV/x-ray (HCX) pulse (red) propagating just in front of the electron layer; (3) the reflected laser pulse leaves to the left, while the HCX followed by the RES exits vertically in the initial direction of the drive pulse.

gets a transverse kick ($p_{y0} = mc \tan \theta$) in the y direction of the RES plane. The corresponding transverse current radiates the unipolar half-cycle pulse.

In the simulated case, an s -polarized laser pulse is incident on target under an angle of $\theta = 30^\circ$. The laser pulse is given by $a(\tau, y) = a_0 \sin^2(\pi\tau/T_L) \exp(-y^2/R_L^2) \cos(2\pi\tau/\tau_L)$ for $0 < \tau < T_L$ with $\tau = t - x/c$, $a_0 = 20$, $\tau_L = \lambda_L/c$, $T_L = 3\tau_L$, and $R_L = 5\lambda_L$. The central intensity is $I_L = 8.55 \times 10^{20}$ W/cm² for wavelength $\lambda_L = 800$ nm. The production layer has electron density $n_e/n_c = 30$ and thickness $d/\lambda_L = 0.001$, the reflector layer $n_e/n_c = 500$ and thickness $d/\lambda_L = 0.05$, where $n_c = 1.74 \times 10^{21}$ cm⁻³ is the critical density for $\lambda_L = 800$ nm. The two layers are separated by $4\lambda_L$ in x direction. The areal electron density of the production foil is $n_e d = 4.17 \times 10^{15}$ cm⁻², corresponding to nano-meshed graphene [11]. Other details on simulation setup are given in the Methods section.

Complete separation of electrons from ions creates an electrostatic field of $E_s = 0.76$ TV/m; it is about two orders of magnitude smaller than the laser electric field of $E_L = 80$ TV/m. In Fig. 2a, one sees how this laser pulse drives the electrons out of the production foil (left panel) and how they pass the reflector in x direction and form of a thin sheet. RES density is plotted for times 7, 14, and $21\tau_L$. The electron sheet is accompanied by a strong unilateral E_y pulse, plotted in the right panel of Fig. 2a at times 14 and $21\tau_L$.

Most important is Fig. 2b, giving line-outs of both electron density n_e (green) and E_y field (red) along the central line ($y = 0$) at times 21 and $60\tau_L$. It shows how the HCX pulse emerges and gradually separates from the electron layer. The maximum field and the width of the HCX pulse are also plotted in Fig. 3a, as they evolve along the propagation coordinate. At $t = 21\tau_L$, the HCX pulse has reached the peak electric field of $E_y/E_0 = 1.75$, corresponding to $E_y = 7$ TV/m and a peak intensity of $I_{HCX} = 1.3 \times 10^{19}$ W/cm². This peak is then slowly falling due to diffraction, while the HCX width is still growing, saturating at $t = 60\tau_L$. Plotted as electric field, the FWHM width of the saturated pulse is 48 as, corresponding to about 24 as, when plotted as intensity. This is the atomic time unit. At $t = 60\tau_L$, the relativistic electron sheet has strongly broadened due to Coulomb expansion, and the peak density of initially $30n_c$ has fallen to $0.2n_c$. Now the HCX pulse has almost separated from the RES and is propagating through vacuum. A remarkable feature is the very sharp front edge, rising from zero to peak values within a few 10 attoseconds. In the present simulation the pulse carries a total energy of 55 μ J, which is about 10^{-4} of the incident laser energy. We have checked that this pulse, about 7 nm long, keeps its half-cycle character over almost a millimeter, before it converts into a single-cycle pulse due to diffraction loss of the long-wavelength components.

Let us now discuss the build-up of transverse current and HCX emission in more detail. The reflector foil plays the key role in switching electron momenta. This is documented in Fig. 3b. It displays γ , γ_x , p_y/mc , and p_z/mc as function of RES position x along the central line $y = 0$. The vertical dashed lines mark the positions of production and reflector foil. It is seen that, during the initial acceleration phase, RES electrons follow qualitatively relativistic single electron motion, which satisfies $\gamma - 1 = p_x/mc = (p_z/mc)^2/2$ and $p_y/mc = 0$ when driven by a planar laser pulse polarized in z direction [14]. When passing the shaded region close to the reflector foil, p_z falls to zero, as the laser amplitude a_z does, and p_y pops up, approaching the predicted value of $p_{y0}/mc = \tan \theta = 0.577$. This behavior is derived in the Methods section. Inside the dense reflector plasma, the transverse current due to p_y is screened, but as soon as it emerges from the rear side, it radiates the HCX pulse, while p_y decreases due to radiation damping. At this point, the present case differs from the photo-conductor pulses, which are mainly emitted

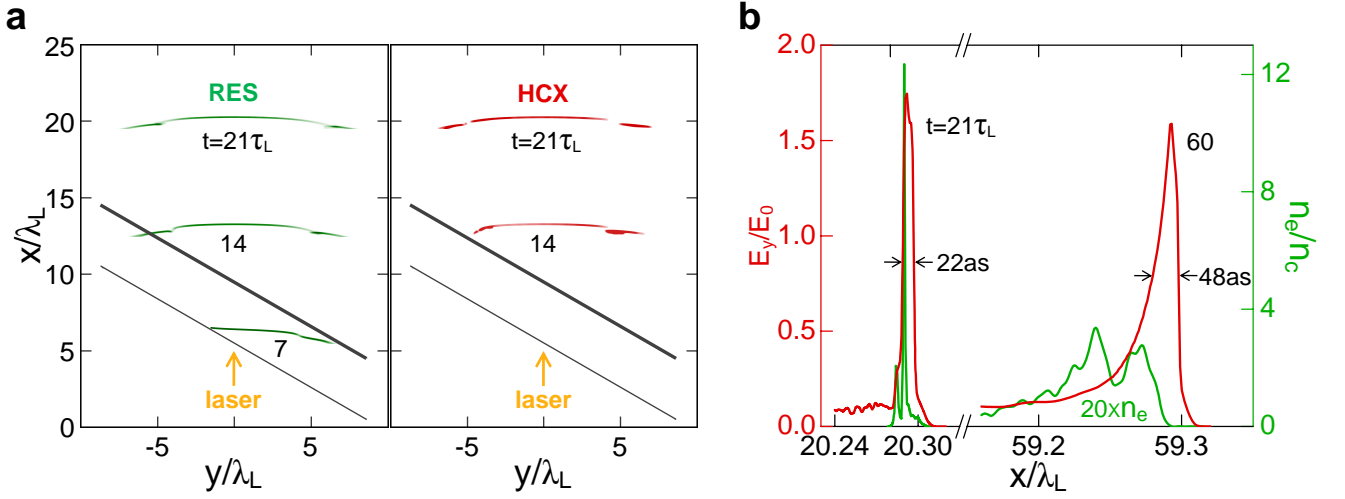


FIG. 2: **Results of 2D PIC simulation.** **a**, Left panel: snapshots of RES in x, y plane plotted as electron density (green) at times 7, 14, and $21\tau_L$; right panel: HCX plotted in terms of E_y (red) at times 14 and $21\tau_L$; the oblique lines indicate production and reflector foil. **b**, Density n_e (in units of critical density $n_c = \epsilon_0 m \omega_L^2 / e^2$) and normalized electric field $a_y = E_y / E_0$ plotted versus x along the central line $y = 0$ at times 21 and $60\tau_L$. Simulation parameters are given in the text and Methods section.

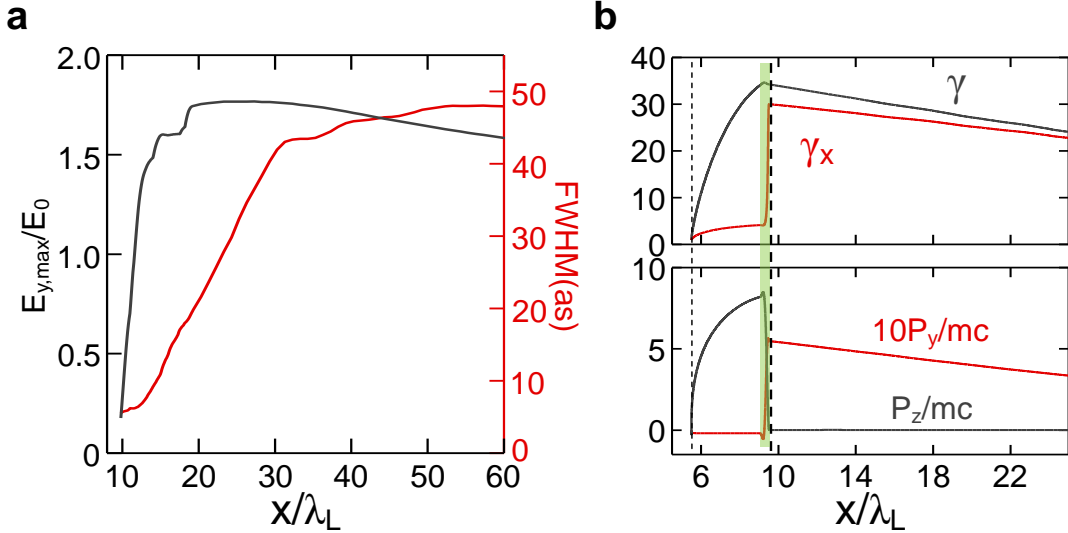


FIG. 3: **Evolution of HCX and RES.** **a**, Evolution of peak electric field $E_{y,max}/E_0$ (black) and FWHM width (red) of the HCX pulse along the propagation coordinate x/λ_L . **b**, Averaged values of γ (black), γ_x (red), p_y/mc (red, scaled by factor 10) and p_z/mc (black) of the RES plotted versus x position. Averages are taken in x direction along the $y = 0$ line. Location of the production foil (thin dashed) is at $x/\lambda_L = 5.5$, and the reflector foil (thick dashed) is at $x/\lambda_L = 9.5$. In the shaded region, electron momenta change due to interaction with the reflected drive laser.

during the build-up phase of the transverse current and have opposite polarity. In Fig. 3b, we have also plotted $\gamma_x = (1 - \beta_x^2)^{-1/2}$, which is related to the full γ by $\gamma = \gamma_x [1 + (p_y/mc)^2 + (p_z/mc)^2]^{1/2}$. One might expect that γ_x stays constant behind the reflector, because there is no further acceleration by the drive laser. However, there is deceleration due to the charge separation field E_s , which still acts behind the reflector. In particular, tail electrons facing the reflector are decelerated, while

front electrons cruise at constant speed. This causes expansion, and a γ_x distribution develops over the sheet. What is actually plotted in Fig. 3b are averages over these distributions.

The electron sheet, moving with γ_x in x direction and having superimposed transverse momentum p_y , emits electromagnetic radiation proportional to the time derivative of the transverse current density in the sheet. In the Methods section, the basic equation is solved

for the idealized case of a uniform zero-thickness RES. Of course, such treatment does not account for finite-size RES dynamics, but provides useful estimates and scalings. The HCX peak electric field is obtained as $E_{max} = \gamma_{x0} E_s \sin \theta = 11$ TV/m for the reference case with the separation field $E_s = 0.76$ TV/m and $\gamma_{x0} = 30$ (see Fig. 3b). It should be compared with the simulated value $E_{max} = 7$ TV/m at $t = 21\tau_L$. In zero-thickness approximation, the HCX has an infinitely sharp front and then decays exponentially with time constant $T \approx mc/(\gamma_{x0} e E_s) = 75$ as, corresponding to a FWHM width of 52 as, which is close to the 48 as, found in Fig. 2b.

Finer details of the HCX front edge and also the HCX growth along the propagation axis, observed in Fig. 3a, are related to the finite size of the RES, when emerging from the reflector. In the simulated density profile at this time, the RES shows two peaks at a distance of $\Delta x_1 \approx 0.008\lambda_L$ and some precursor foot extending over $\Delta x_2 \approx 0.03\lambda_L$. The precursor maps directly into the HCX front edge rising over almost the same distance Δx_2 . Also the propagation distance for saturating the peak HCX field can be estimated as $L_{sat} = \Delta x_1/(1 - \beta_x) \approx 2\gamma_x^2 \Delta x_1 \approx 14\lambda_L$, in fair agreement with Fig. 3a. Here L_{sat} is the distance over which the light signal emitted from the second density peak has to travel to catch up with the first peak. These two major HCX contributions then add up coherently and form the peak of the pulse. Due to retardation the front contribution is already somewhat damped, and this may explain why the peak field of 7 TV/m is lower than the model result of 11 TV/m. It is important to notice that the HCX contributions emitted from different RES layers add up coherently. The coherence is the reason why a major part of the energy deposited in the transverse RES current is actually radiated, even when the RES has substantially expanded.

In conclusion, we have found an efficient new option to generate single attosecond pulses. It involves a double foil target to produce and purify a RES. Under oblique incidence, it radiates a half-cycle pulse of a few 10 as duration with peak electric field up to 10^{13} V/m and pulse energies up to the 0.1 mJ level. The laser-to-HCX conversion efficiency amounts to a few 10^{-4} . Most important for experiments is the extremely sharp front edge with rise times of a few 10 as. HCX properties and scaling relations have been derived in simple analytical terms. Compared to Thomson scattering as a way to generate single attosecond pulses [13], the present method is simpler to implement, because only a single laser beam is required. It is hoped that the present paper will stimulate experiments.

Methods

Transverse momentum. For oblique incidence, electron dynamics close to the reflector are quite complex. A simple analytic approach is possible when transforming to a frame in which the laser beam is vertically incident as

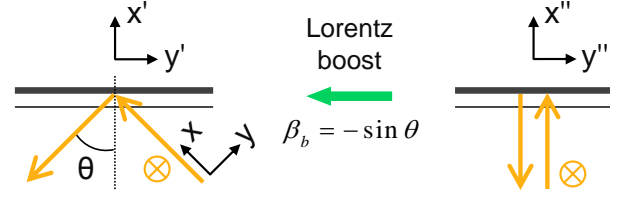


FIG. 4: Definition of coordinate transformations.

depicted in Fig. 4 [15]. First rotating the x, y beam frame to the x', y' layer frame and then applying a Lorentz-boost in y' direction with $\beta_b = -\sin \theta$, $\gamma_b = \sec \theta$, electron energy-momentum $(\gamma, \hat{p}_x, \hat{p}_y, \hat{p}_z)$ transforms to $(\gamma'', \hat{p}_x'', \hat{p}_y'', \hat{p}_z'')$ with $\gamma'' = (1 + \hat{p}_x'^2 + \hat{p}_y'^2 + \hat{p}_z'^2)^{1/2}$; here energy is in units mc^2 and momenta in mc . Due to conservation of canonical momentum, the z -component of momentum (vertical to the plane of Fig. 4) is invariant and equals the vector potential a_z for s-polarized light, $\hat{p}_z = \hat{p}_z' = \hat{p}_z'' = a_z$. In the boosted frame, also the y -component $\hat{p}_y'' = \beta_b \gamma_b = \tan \theta$ is conserved. Transforming back to the lab frame, we find

$$\hat{p}_y = \hat{p}_y'' + (\hat{p}_x'' - \gamma'') \sin \theta \quad (1)$$

with $\hat{p}_x'' - \gamma'' = \hat{p}_x'' - (1 + \tan^2 \theta + \hat{p}_x''^2 + a_z^2)^{1/2}$. Here we notice that, behind the reflector where $a_z = 0$, we have $\hat{p}_x'' - \gamma'' \rightarrow 0$ for relativistic electrons, provided that $\hat{p}_x'' \cos \theta \gg 1$. In this case, one has $\hat{p}_y \approx \hat{p}_y'' = \tan \theta$, stating that electrons emerge from the reflector with non-zero momentum in the direction of the RES plane. Momentum transfer into y -direction occurs within a narrow region close to the reflector (see Fig. 3b), where $a_z \rightarrow 0$.

Scaling of HCX emission. HCX generation from a RES can be described by the one-dimensional wave equation

$$(\partial^2/\partial x^2 - c^{-2}\partial^2/\partial t^2)E_y = \varepsilon_0^{-1}c^{-2}\partial J_y/\partial t, \quad (2)$$

where $J_y = -ec\beta_y n_e$ is the radiating current. The solution can be written as $E_y(x, t) = -(2\varepsilon_0 c)^{-1} \int \int dx' dt' H(t - t' - |x - x'|/c) \partial J_y(x', t')/\partial t'$, where $H(t)$ is the step function. For analytical treatment, the difficulty is that $J_y(x, t)$ is a complicated function of space and time in general. Here we restrict ourselves to a RES of zero-thickness, approximating the density profile as $n(x) = n_e \delta(x/d)$ with finite areal density $\int n(x) dx = n_e d$, and first consider the rest frame (index R), choosing uniform velocity $\beta_{xR} = 0$ and $\beta_{yR0} = \sin \theta$ initially. The solution consists of two half-cycle electromagnetic pulses emitted symmetrically in $\pm x$ direction, just as observed in the photon-conductor experiments [4]. Expressing J_y in terms of transverse momentum p_y , we find for the wave traveling in $+x$ direction

$$E_{yR}(\tau_R) = (E_s/2)p_y(\tau_R)/(mc\gamma_y), \quad (3)$$

where $\tau_R = t - x/c$ and $E_s = en_e d/\epsilon_0$. The relativistic factor $\gamma_y = \sqrt{1 + (p_y/mc)^2}$ can be estimated as $\gamma_y \approx 1$. At $x = 0$ (i.e. $\tau_R = t$), where the layer is located, E_{yR} damps electron momentum according to $dp_y/dt = -eE_{yR}(t)$. One finds that both $p_y(t)$ and the emitted pulse $E_{yR}(\tau_R)$ decay exponentially on time scale $T_R = 2mc/(eE_s)$. These results apply to the rest frame of the layer. Performing a Lorentz-transformation to the lab frame, in which the layer is moving with velocity $c\beta_x$ and $\gamma_x = (1 - \beta_x^2)^{-1/2}$ in normal direction, we find the coordinate of the forward HCX pulse $\tau = \gamma_x(1 - \beta_x)\tau_R \approx \tau_R/(2\gamma_x)$ and the electric field $E_y = \gamma_x(1 + \beta_x)E_{yR} \approx 2\gamma_x E_{yR}$. The maximum HCX field scales like $E_{max} \propto \gamma_x E_s \sin \theta$ and the pulse width like $T \propto (\gamma_x E_s)^{-1}$.

PIC simulation. We have carried out all simulations using the JPIC code [16], which employs a field

solver free of numerical dispersion in x direction [17]. Since an isolated HCX pulse contains extremely broad frequency components, for accurately simulating HCX generation and propagation, it is crucial to use such kind of dispersion-free field solver. The simulation box has a size $25\lambda_L \times 20\lambda_L$ in the xy plane. Moving window technique is used to extend the simulation distance. There are 1000 cells and 400 cells per λ_L in x and y directions, respectively. Along the central line $y = 0$, the undersides of both foils are at $x = 5.5\lambda_L$ and $9.5\lambda_L$, respectively. We use 3×10^7 and 1×10^7 macro-particles in the production and reflector foils, respectively. Ions in both layers are immobile. An initial electron temperature of 10 eV is taken for the production sheet to mimic ionization, while the reflector foil is initialized as cold plasma with zero temperature. The drive laser begins to enter the simulation box from the lower boundary ($x = 0$) at $t = 0$.

-
- [1] Krausz, F. & Ivanov, M. Attosecond physics. *Rev. Mod. Phys.* **81**, 163-234 (2009).
 - [2] Goulielmakis, E. *et al.* Single-cycle nonlinear optics. *Science* **320**, 1614-1617 (2008).
 - [3] Tsakiris, G.D., Eidmann, K., Meyer-ter-Vehn, J. & Krausz, F. Route to intense single attosecond pulses. *New J. Phys.* **8**, 19 (2006).
 - [4] You, D., Jones, R.R., Bucksbaum, P.H. & Dykaar, D.R. Generation of high-power sub-single-cycle 500-fs electromagnetic pulses. *Opt. Lett.* **18**, 290-292 (1993).
 - [5] Jones, R.R., You, D. & Bucksbaum, P.H. Ionization of Rydberg atoms by half-cycle electromagnetic pulses. *Phys. Rev. Lett.* **70**, 1236-1239 (1993).
 - [6] Bratman, V.L., Jaroszynski, D.A., Samsonov, S.V. & Saviolov, A.V. Generation of ultra-short electromagnetic pulses from quasi-planar electron bunches. *Nucl. Instr. and Meth. A* **475**, 436-440 (2001).
 - [7] Herrmann, D. *et al.* Generation of sub-three-cycle, 16 TW light pulses by using noncollinear optical parametric chirped-pulse amplification. *Opt. Lett.* **34**, 2459-2461 (2009).
 - [8] Mikhailova, J.M. *et al.* Ultra-high-contrast few-cycle pulses for multipetawatt-class laser technology. *Opt. Lett.* **36**, 3145-3147 (2011).
 - [9] Dromey, B. *et al.* High harmonic generation in the relativistic limit. *Nature Phys.* **2**, 456-459 (2006).
 - [10] Geim, A.K. & Novoselov, K.S. The rise of graphene. *Nature Mater.* **6**, 183-191 (2007).
 - [11] Bai, J., Zhong, X., Jiang, S., Huang, Y. & Duan, X. Graphene nanomesh. *Nature Nanotech.* **5**, 190-194 (2010).
 - [12] Meyer-ter-Vehn, J. & Wu, H.-C. Coherent Thomson backscattering from laser-driven relativistic ultra-thin electron layers. *Eur. Phys. J. D* **55**, 433-441 (2009).
 - [13] Wu, H.-C., Meyer-ter-Vehn, J., Fernandez, J. & Hegelich, B.M. Uniform laser-driven relativistic electron layer for coherent Thomson scattering. *Phys. Rev. Lett.* **104**, 234801 (2010).
 - [14] Meyer-ter-Vehn, J., Pukhov, A. & Sheng, Z.-M. *Relativistic laser plasma interaction, in atoms, solids and plasmas in super-intense laser fields*, edited by Batani D. *et al.* (Kluwer Academic/Plenum Publishers, 2001).
 - [15] Bourdier, A. Oblique incidence of a strong electromagnetic wave on a cold inhomogeneous electron plasma. Relativistic effects. *Phys. Fluids* **26**, 1804-1807 (1983).
 - [16] Wu, H.-C. JPIC & How to make a PIC code. Preprint at <http://arxiv.org/abs/1104.3163> (2011).
 - [17] Sentoku, Y. & Kemp, A.J. Numerical methods for particle simulations at extreme densities and temperatures: Weighted particles, relativistic collisions and reduced currents. *J. Comp. Phys.* **227**, 6846-6861 (2008).

Acknowledgments

This work is supported by the LDRD Program 20110341ER at the Los Alamos National Laboratory. J. Meyer-ter-Vehn was supported by the Munich Center for Advanced Photonics and by the Association EURATOM-Max-Planck-Institute for Plasma Physics. H.-C. Wu is grateful for supports from Dr. J. Fernandez and Dr. B.M. Hegelich.

Author contributions

H.-C.W. discovered the new effect described in this paper, he carried out all simulations and developed the basic theory. J.M.-t.-V. wrote the paper and clarified some details of the physics. Both authors take full responsibility for the results presented.

Additional information

The authors declare no competing financial interests. Correspondence and requests for materials should be addressed to H.-C.W.